PHYSICAL REVIEW C **96**, 064608 (2017)

Cluster formation in precompound nuclei in the time-dependent framework

B. Schuetrumpf[1,2,3] and W. Nazarewicz[4]

[1]*Institut für Kerphysik, Technische Universität Darmstadt, Schlossgartenstraße 2, 64289 Darmstadt, Germany*

[2]*GSI Helmholzzentrum für Schwerionenforschung, Planckstraße 1, 64291 Darmstadt, Germany*

[3]*FRIB Laboratory, Michigan State University, East Lansing, Michigan 48824, USA*

[4]*Department of Physics and Astronomy and FRIB Laboratory, Michigan State University, East Lansing, Michigan 48824, USA*

(Received 2 October 2017; published 15 December 2017)

Background: Modern applications of nuclear time-dependent density functional theory (TDDFT) are often capable of providing quantitative description of heavy ion reactions. However, the structures of precompound (preequilibrium, prefission) states produced in heavy ion reactions are difficult to assess theoretically in TDDFT as the single-particle density alone is a weak indicator of shell structure and cluster states.

Purpose: We employ the time-dependent nucleon localization function (NLF) to reveal the structure of precompound states in nuclear reactions involving light and medium-mass ions. We primarily focus on spin saturated systems with $N = Z$. Furthermore, we study reactions with oxygen and carbon ions, for which some experimental evidence for α clustering in precompound states exists.

Method: We utilize the symmetry-free TDDFT approach with the Skyrme energy density functional UNEDF1 and compute the time-dependent NLFs to describe ^{16}O + ^{16}O, ^{40}Ca + ^{16}O, ^{40}Ca + ^{40}Ca, and ^{16,18}O + ^{12}C collisions at energies above the Coulomb barrier.

Results: We show that NLFs reveal a variety of time-dependent modes involving cluster structures. For instance, the ^{16}O + ^{16}O collision results in a vibrational mode of a quasimolecular α-^{12}C-^{12}C-α state. For heavier ions, a variety of cluster configurations are predicted. For the collision of ^{16,18}O + ^{12}C, we showed that the precompound system has a tendency to form α clusters. This result supports the experimental findings that the presence of cluster structures in the projectile and target nuclei gives rise to strong entrance channel effects and enhanced α emission.

Conclusion: The time-dependent nucleon localization measure is a very good indicator of cluster structures in complex precompound states formed in heavy-ion fusion reactions. The localization reveals the presence of collective vibrations involving cluster structures, which dominate the initial dynamics of the fusing system.

DOI: 10.1103/PhysRevC.96.064608

I. INTRODUCTION

Low-energy fusion initiated by light and medium-mass ions is of great importance for both basic science and applications. In many cases, this process can be well described in terms of the compound nucleus framework, which assumes that the excited composite nucleus formed in the fusion reaction lives long enough for thermodynamic equilibrium to be established. In many cases, however, entrance channel effects can be significant, and an idealized picture of a compound nucleus, which is not expected to retain memory of how it was formed, is clearly not appropriate [1–4].

In this work, we carry out theoretical study of entrance channel effects in low-energy collisions of light heavy-ions using the time-dependent density functional theory (TDDFT) approach. In particular, we are interested in the structure of nuclear configurations formed shortly following fusion. Those are precompound (or preequilibrium or prefission) nuclear states formed in fusion or fusion-fission reactions that carry significant memory of the entrance channel.

The self-consistent time-dependent Hartree-Fock theory, or its TDDFT extension, is a standard tool to study heavy-ion collisions (see Refs. [5–9] for reviews). Advanced symmetry-unrestricted TDDFT calculations for nuclear reactions and other large-amplitude collective motion have been dramatically advanced by the use of high-performance computing [10–22]. A useful extension of TDDFT is density constrained TDHF [23,24], which can be used to extract capture cross sections, including the sub-barrier regime.

The structure of precompound states formed in fusion reactions can be impacted by the presence of clustering effects. Indeed, clustering has been shown to be very important theoretically in low-energy [25] and high-energy heavy-ion collisions [26,27]. Moreover, there exists some experimental evidence, as well as quite a few theoretical predictions, for the presence of nuclear molecular states in light and medium-mass nuclei at high excitation energy [28–34].

To study clustering effects in heavy-ion fusion reactions, we utilize a measure called the fermion localization function, originally developed for electronic calculations [35]. As demonstrated in Refs. [36–38], the nucleon localization function (NLF) is an excellent tool to reveal shell and cluster effects in nuclei. In this work, we apply the concept of nuclear localization to analyze the structure of states formed in heavy-ion collision TDDFT simulations. In this way, we can quantify the nature of preequilibrium configurations whose structure is largely undiagnosed when using conventional techniques.

This article is organized as follows. Section II contains a brief description of the TDDFT formalism used in this work and describes nucleon localization functions. In Sec. III we analyze the symmetric collisions of the doubly magic nuclei ^{16}O + ^{16}O and ^{40}Ca + ^{40}Ca, while in Sec. IV we discuss the

asymmetric collisions of ^{16}O + ^{40}Ca and ^{16,18}O + ^{12}C. Finally, the summary and outlook are provided in Sec. V.

II. THEORETICAL FRAMEWORK

A. Nuclear TDDFT

For the TDDFT calculations we utilize the software package SKY3D [39], which solves the time-dependent Hartree-Fock equations in the coordinate space on an equidistant grid using fast Fourier transforms (FFTs) for derivatives. For the nuclear mean field, we use the Skyrme functional UNEDF1 [40], which is expected to perform well at large deformations. UNEDF1 has been optimized to selected properties of nuclei and nuclear matter and no additional parameters have been introduced for the time-dependent calculations presented in this work.

The initial wave functions of colliding ions are determined from ground-state (g.s.) DFT calculations performed with SKY3D. For closed-shell systems, pairing correlations are ignored. For the open-shell systems ^{18}O and ^{12}C, we use the BCS pairing as in Ref. [41]. In the time-dependent calculations we use the frozen occupation approximation.

The wave functions of two colliding ions are combined into one Slater determinant by orthogonalizing all single-particle wave functions. The fragments are boosted by multiplying the wave functions with a complex phase factor and then evolved in time with a finite time step of 0.2 fm/c. The SKY3D framework does not impose any symmetry restrictions. However, while the long-range Coulomb problem is solved for open boundary conditions, the short-range nuclear interaction is determined in the box with periodic boundary conditions, since the FFT approach is used for computing derivatives. We took a cubic box with a large length of 32 fm to ensure that the wave functions vanish at the boundaries. Finite-volume effects can be practically eliminated using the twist-averaged boundary condition [22,42]. However, due to the relatively small time scales considered, such an approach was not needed in this work.

While TDDFT calculations can well reproduce certain observables such as the fusion, or capture, cross sections above the Coulomb barrier, there are obvious limitations to the theory, such as its inability to describe the motion of the system in the classically forbidden region, many-body dissipation, and fluctuations due to internally broken symmetries [43]. In particular, the transition to the compound-nucleus phase cannot be described within TDDFT. In this study, therefore, we shall limit our investigations to the precompound configurations involving relatively short time scales.

B. Nucleon localization function

The electron localization function was originally proposed to characterize chemical bonding in electronic systems [35,44–48]. Subsequently, the nucleon localization function (NLF) was applied to atomic nuclei to visualize cluster structures in light systems [36,38]. The NLF is derived from the inverse of the conditional probability of finding a nucleon of isospin q (n or p) in the vicinity of another nucleon of the same isospin and signature quantum number σ (= ↑ or ↓), knowing with certainty that the latter particle is located at position $\boldsymbol{r}$. The NLF can entirely be expressed through the local DFT densities:

$$\mathcal{C}_{q\sigma}(\boldsymbol{r}) = \left[1 + \left(\frac{\tau_{q\sigma}\rho_{q\sigma} - \frac{1}{4}|\nabla\rho_{q\sigma}|^2 - \boldsymbol{j}_{q\sigma}^2}{\rho_{q\sigma}\tau_{q\sigma}^{\mathrm{TF}}}\right)^2\right]^{-1}, \quad (1)$$

where $\rho_{q\sigma}$, $\tau_{q\sigma}$, $\boldsymbol{j}_{q\sigma}$, and $\nabla\rho_{q\sigma}$ are the particle density, kinetic energy density, current density, and density gradient, respectively, and $\tau_{q\sigma}^{\mathrm{TF}}$ denotes the Thomas-Fermi kinetic energy.

In Ref. [36] mostly $N = Z$ nuclei up to $A = 20$ have been studied. It was demonstrated that α clusters tend to appear at the tips of deformed nuclei, and that ^{12}C clusters can be revealed through characteristic rings of an enhanced NLF. Furthermore, NLFs have also been studied to investigate fragment formation during nuclear fission of heavy nuclei [37], and also to investigate pasta phases in the inner crust of neutron stars [38].

While in g.s. calculations for even-even nuclei the time-reversal symmetry is conserved and the current density $\boldsymbol{j}_{q\sigma}$ vanishes, it becomes an important ingredient in time-dependent calculations. Furthermore, since in this work we are primarily interested in the localization of neutrons and protons, and not in the signature content, in the following we consider signature-average densities, such as $\rho_q = (\rho_{q\uparrow} + \rho_{q\downarrow})/2$.

To study α clusters or clusters of α-conjugate nuclei in light-to-medium $N = Z$ systems with weak Coulomb forces, it is convenient to utilize the α-NLF as introduced in Ref. [36]:

$$\mathcal{C}_\alpha = \sqrt{\mathcal{C}_n\mathcal{C}_p}. \quad (2)$$

The localization function takes generally values between 0 and 1. High values of NLF indicate that the probability of finding two particles (of the same type) close to each other is low. Since the localization function (1) is normalized to the Thomas-Fermi kinetic energy, the value of $\mathcal{C} = 1/2$ corresponds to a limit of the homogeneous Fermi gas, in which the individual orbits are spatially delocalized.

Examples of the density distribution and corresponding localizations $\mathcal{C}_\alpha$ predicted in TDDFT are shown in Fig. 1. In general, particle densities contain little information about the internal structure of the system. On the other hand, the NLFs reveal distinct regions with enhanced localization that signal the appearance of cluster structures. Regions where clusters overlap exhibit decreased localization. In the following, we shall use localizations $\mathcal{C}_\alpha$ to identify and visualize various cluster structures and their collective motion.

C. Assessing nucleon content in clusters

To complement the analysis based on NLFs, we extract the nucleon content in the spatial regions dominated by single clusters. Such regions correspond to enhanced values of localization; they are separated by areas of $\mathcal{C}_\alpha \approx 0.5$ in which the cluster wave functions overlap. For simplicity, we only consider central collisions and assume that the clusters are located along the direction of the boost (z axis). The nucleon

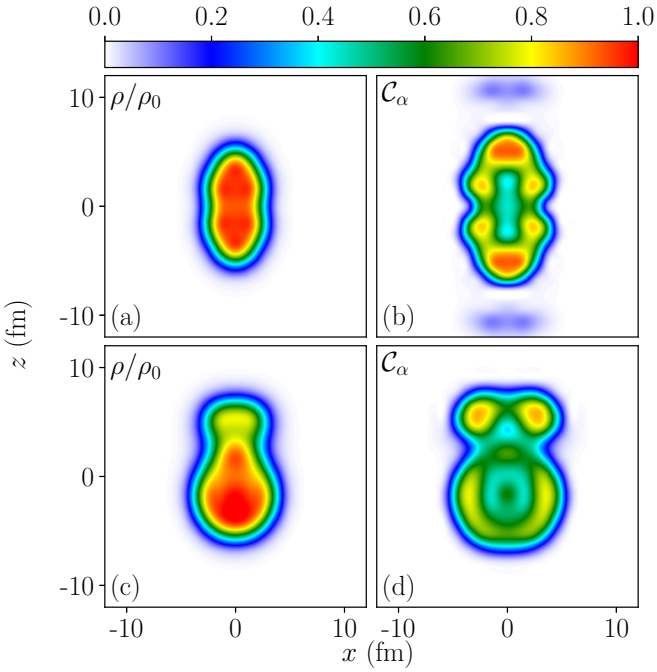

FIG. 1. Snapshots of ^{16}O + ^{16}O (top) and ^{16}O + ^{40}Ca (bottom) TDDFT collision simulations. Total densities normalized to the nuclear saturation density $\rho_0 = 0.16$ fm^{-3} are shown in the left panels while the corresponding localizations $\mathcal{C}_\alpha$ are displayed in the right panels. Since the collisions are central, axial symmetry with respect to the z axis is conserved.

content of a cluster identified by means of the NLF is given by

$$A(z_1,z_2) = \iint dx\,dy \int_{z_1}^{z_2} \rho(x,y,z)dz. \tag{3}$$

The NLF offers some freedom to chose the values of z_1 and z_2. Here, we chose the values such that $A(z_1,z_2)$ is an integer.

III. LOCALIZATION IN SYMMETRIC COLLISIONS

A. ^{16}O + ^{16}O collisions

We begin with the case of the symmetric central collision of two ^{16}O nuclei with energy $E_{\rm cm} = 20$ MeV just above the barrier. As seen in the $t = 50$ fm/c panel of Fig. 2, the g.s. localization of ^{16}O exhibits characteristic pattern of concentric rings, which can be associated with the filling of $0s$ and $0p$ shells.

As the fragments come closer, the magnitude of the NLF of the fragments facing each other gets reduced, because the outer parts of the wave functions of the fragments overlap. At $t = 150$ fm/c a precompound nucleus is formed. At later times, the system reveals strong α clustering. As shown in the supplemental material, the precompound nucleus oscillates predominantly between the structures shown in the $t = 240$ fm/c and $t = 330$ fm/c panels, going through the intermediate states displayed in $t = 190$ fm/c and $t = 280$ fm/c panels.

The configuration at $t = 240$ fm/c exhibits two rings of enhanced localization at $z = \pm 4$ fm. As already mentioned in

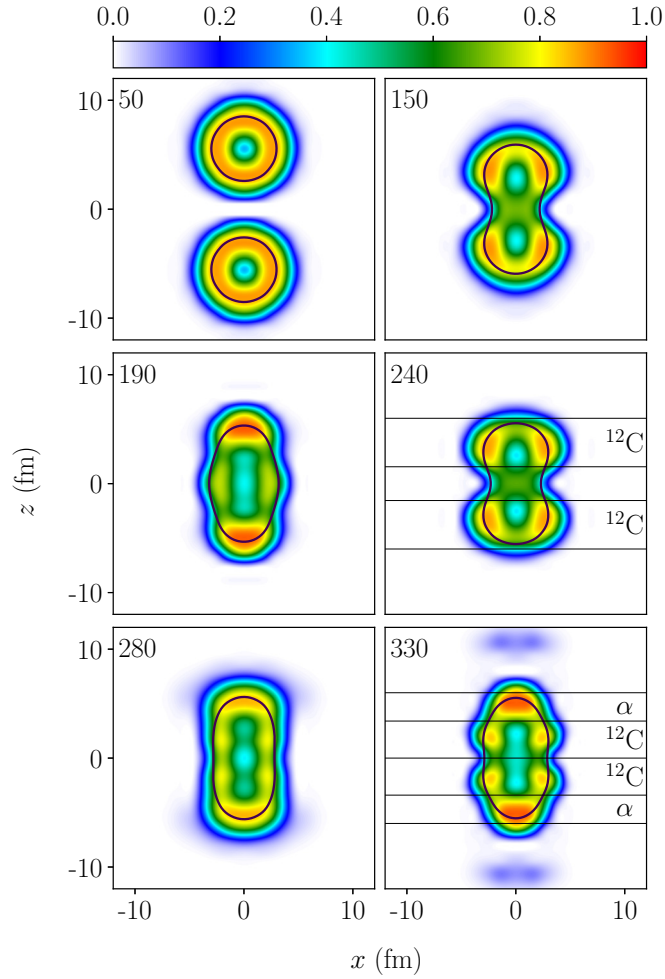

FIG. 2. Localization $\mathcal{C}_\alpha$ for the central collision of ^{16}O + ^{16}O at $E_{\rm cm} = 20$ MeV. The numbers indicate the collision time (in fm/c). The black line marks the $\rho = 0.05$ fm^{-3} contour of the total density. See Supplemental Material [49] for animations.

Ref. [36], these rings can be interpreted as oblate-deformed ^{12}C clusters. Indeed, the nucleon content (3) corresponding to the regions marked by horizontal lines in Fig. 2 matches nicely the NLF ring structure. The central region between the two ^{12}C clusters contains four neutrons and four protons. The structure at $t = 330$ fm/c exhibits large localization at the tips, which is indicative of α clustering. The interior is made of two ring structures, which we interpret as ^{12}C oblate clusters; the nucleon content is consistent with this interpretation. We can thus view the precompound state depicted in Fig. 2 as a collective oscillation of two ^{12}C rings against two α clusters.

At higher center-of-mass energies, the system is expected to fission into two symmetric fragments following a brief intermediate phase. An example of a such fusion-fission (or quasifission) reaction is shown in Fig. 3, which illustrates the ^{16}O + ^{16}O collision at $E_{\rm cm} = 100$ MeV. Following the initial contact ($t = 50$ fm/c), the intermediate state is formed that eventually splits up at $t = 240$ fm/c. In the intermediate state, two ^{12}C clusters are visible at the tips and the α clusters are formed in the neck area. Following fission, the highly excited

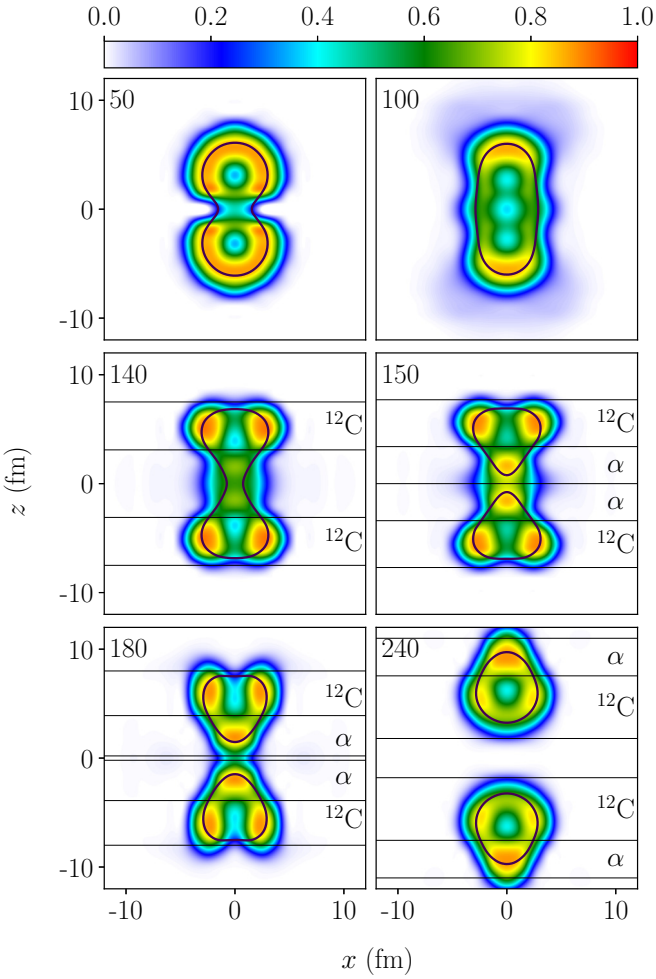

FIG. 3. Similar to Fig. 2 except for $E_{\rm cm} = 100$ MeV.

^{16}O nuclei undergo octupole vibrations, in which the α cluster oscillates with respect to the ^{12}C cluster.

In peripheral collisions with a nonzero impact parameter different clusters are also predicted. Figure 4 shows the NLF contour plots in three dimensions for the α-^{12}C-^{12}C-α molecular state found in Fig. 2 at $t = 330$ fm/c for three values of the impact parameter. While for the central collision the system conserves axial symmetry, for $b > 0$ the α clusters

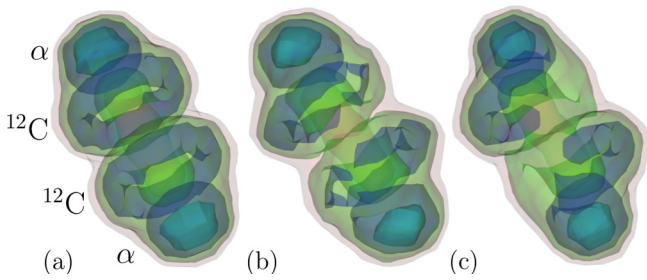

FIG. 4. The α-^{12}C-^{12}C-α structure formed at $t = 330$ fm/c in ^{16}O + ^{16}O collision at $E_{\rm cm} = 20$ MeV for three values of the impact parameter: $b = 0$ fm (a), $b = 2$ fm (b), and $b = 4$ fm (c). The color scale is 0.55 light red, 0.65 green, 0.75 blue, and 0.85 cyan.

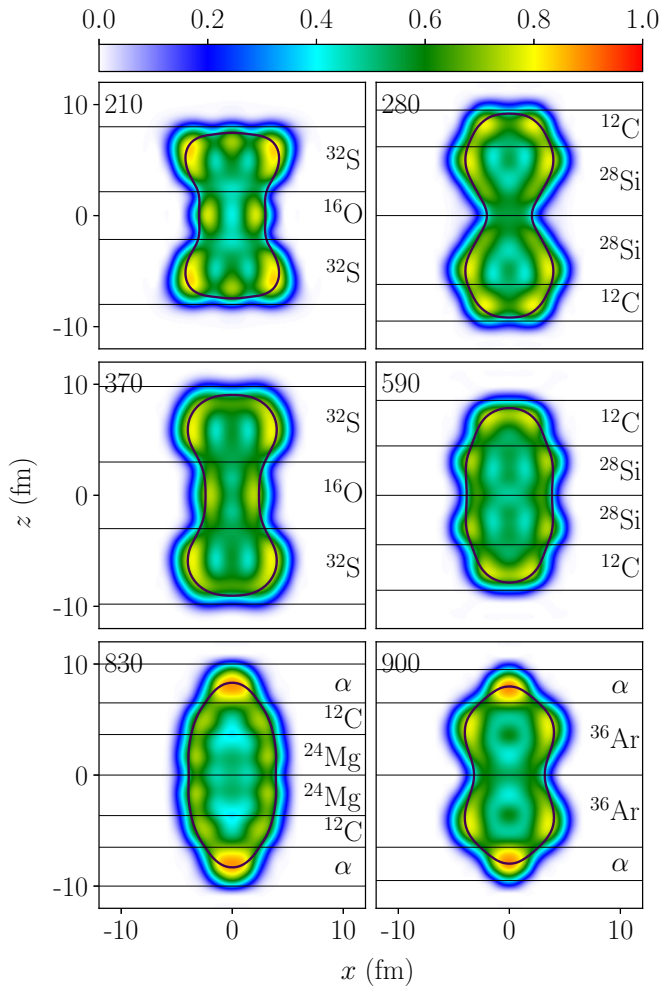

FIG. 5. Similar to Fig. 2 except for the central collision of ^{40}Ca + ^{40}Ca at $E_{\rm cm} = 150$ MeV. See Supplemental Material [49] for animations.

shift slightly into the direction of rotation, thus creating more overlap between α and ^{12}C clusters. A similar situation is expected for other configurations.

B. ^{40}Ca + ^{40}Ca collisions

The precompound, or prefission, states produced in ^{16}O + ^{16}O collisions are expected to have a fairly simple cluster makeup. This is not going to be the case as one moves up in mass to heavier projectiles and targets. A case in point is the collision of doubly-magic ^{40}Ca nuclei. Figure 5 shows the results of TDDFT simulations for the precompound state formed in ^{40}Ca + ^{40}Ca central collision at at $E_{\rm cm} = 150$ MeV. In contrast to the simple ^{16}O + ^{16}O case, the resulting excited configuration of ^{80}Zr exhibits a rather intricate structure involving a variety of clusters and shapes as time evolves. While in the ^{16}O collision the α and ^{12}C clusters can be clearly identified through NLFs, this does not hold in general for the heavier case.

At early times, $t = 210$ fm/c and $t = 370$ fm/c, the precompound state can be associated with configurations

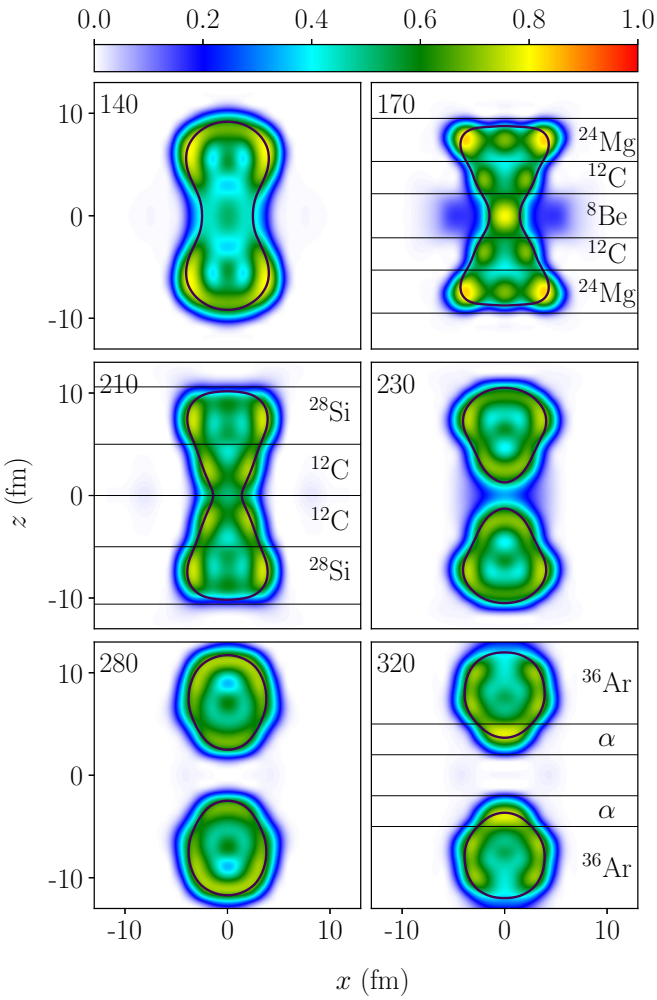

FIG. 6. Similar to Fig. 5 except for $E_{\rm cm} = 300$ MeV.

involving two ^{32}S clusters separated by a smaller inner cluster of ^{16}O. The shapes at $t = 280$ fm/c and $t = 590$ fm/c consist of two smaller ^{12}C clusters at the tips and two ^{28}Si clusters in the interior. At later times, however, the picture changes as a pronounced α clustering appears at the tips. At $t = 830$ fm/c, four rings of enhanced localization are visible within the nuclear volume. The outer rings have the ^{12}C content while the inner ones can be associated with ^{24}Mg. At $t = 900$ fm/c the system resembles an α-^{36}Ar-^{36}Ar-α molecular state. As shown in the Supplemental Material [49], at $t > 1000$ fm/c the the system remains in a superdeformed shape, with the inner cluster structures evolving continuously.

In Fig. 6 we show the fusion-fission of ^{40}Ca + ^{40}Ca at $E_{\rm cm} = 300$ MeV. Here, the intermediate state survives for only a very short time before the system splits up. At $t = 170$ fm/c, oblate ^{24}Mg clusters are visible at the tips. They are separated by two ^{12}C clusters and the region of enhanced localization in the center associated with ^{8}Be. The enhanced localization in the center vanishes at $t = 210$ fm/c and only ^{28}Si and ^{12}C cluster structures remain. After the breakup, the fragments undergo parity-breaking oscillations

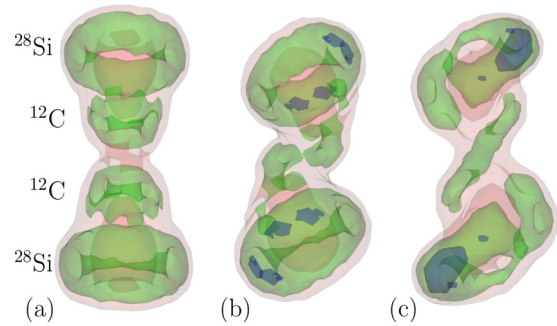

FIG. 7. NLF in collision of ^{40}Ca + ^{40}Ca at $E_{\rm cm} = 300$ MeV for three values of the impact parameter: $b = 0$ fm at $t = 210$ fm/c (a); $b = 3$ fm at $t = 210$ fm/c (b); and $b = 6$ fm at $t = 460$ fm/c (c).

along the z direction. As seen in the $t = 320$ fm/c panel, this octupole mode can be viewed as a vibration of the ^{36}Ar-α quasimolecule.

To complete the discussion, in Fig. 7 we show the NLFs for the peripheral ^{40}Ca + ^{40}Ca collision at $E_{\rm cm} = 300$ MeV

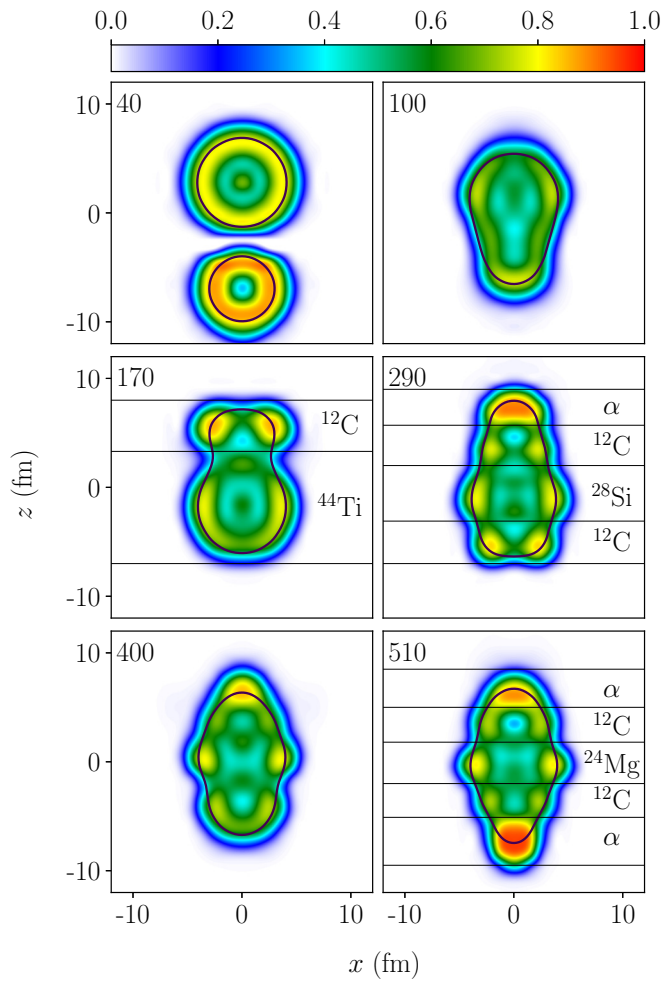

FIG. 8. Similar to Fig. 2 except for the central collision of ^{16}O + ^{40}Ca at $E_{\rm cm} = 80$ MeV. See Supplemental Material [49] for animations.

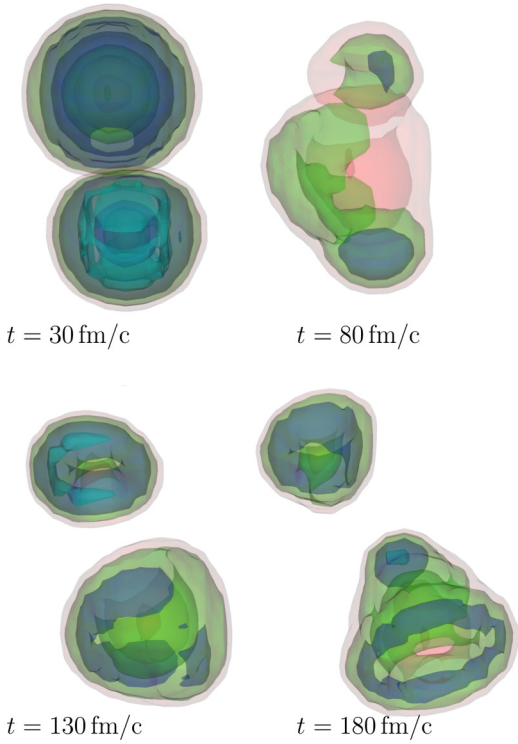

FIG. 9. NLF $\mathcal{C}_\alpha$ for the ^{16}O + ^{40}Ca collision of at $E_{\rm cm} = 200$ MeV and $b = 2$ fm at different times, as indicated.

just before the system's breakup. The situation resembles the results for ^{16}O + ^{16}O in Fig. 4. Namely, the rings of enhanced localization become tilted and partly overlap at increasing values of the impact parameter.

IV. LOCALIZATION IN ASYMMETRIC COLLISIONS

A. ^{16}O + ^{40}Ca

For asymmetric collisions, the precompound state is reflection asymmetric and its cluster content becomes fairly complex. The NLFs for the central ^{16}O + ^{40}Ca collision at $E_{\rm cm} =$ 80 MeV are shown in Fig. 8. A precompound state is formed at $t = 100$ fm/c. At $t = 170$ fm/c, a quasimolecular ^{12}C-^{44}Ti structure is predicted. At later times, the system undergoes large-amplitude vibrations involving different quasimolecular configurations with oblate ^{28}Si and ^{24}Mg clusters as well as intermediate states that do not exhibit a compelling cluster structure.

An interesting case is the ^{16}O + ^{40}Ca collision at $E_{\rm cm} =$ 200 MeV with an impact parameter of $b = 2$ fm. Due to the asymmetry of the collision, the final fragments have different numbers of neutrons and protons. In this case, shown in Fig. 9, the composite system formed at $t =$ 80 fm/c splits up after approximately $t = 150$ fm/c. The mass number of the lighter fragment is $A \approx 13.7$ and its charge number is $Z \approx 7$. The snapshots at $t = 130$ fm/c and $t =$ 180 fm/c indicate a contribution of ^{12}C cluster in the lighter fragment.

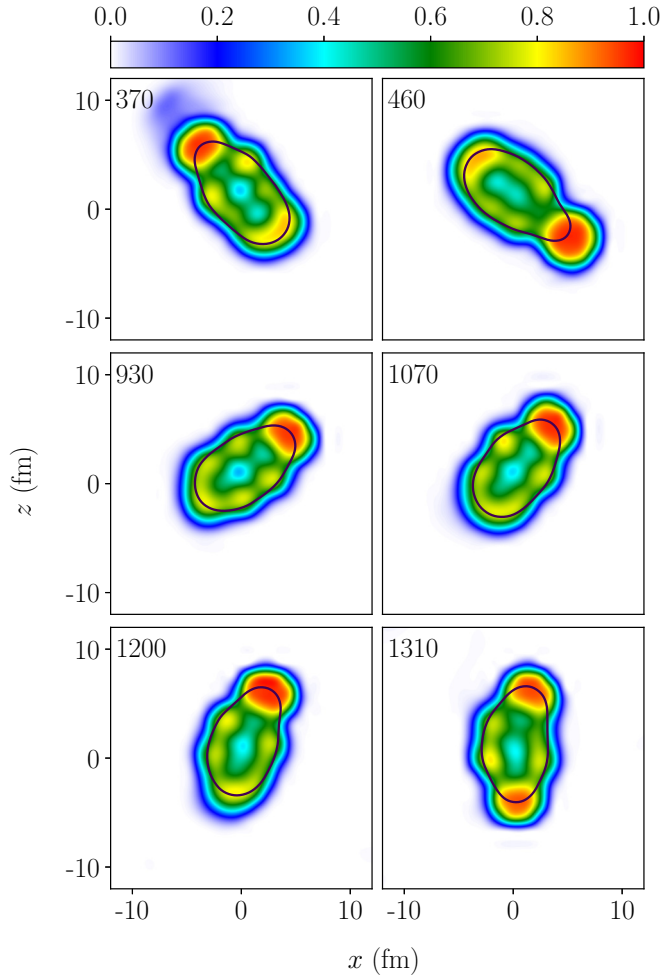

FIG. 10. Similar to Fig. 2 except for the ^{18}O + ^{12}C collision at $E_{\rm cm} = 14$ MeV and $b = 2$ fm. See Supplemental Material [49] for animations.

B. ^{16,18}O + ^{12}C

The ^{16}O + ^{12}C, ^{16}O + ^{13}C, and ^{18}O + ^{12}C collisions were studied experimentally in Refs. [4,50–52]. (We note that a strong α transfer in reactions with ^{18}O has been observed [53,54].) In particular, in Ref. [4] the cross sections for α decays following fusion at energies around the fission barrier (6–14 MeV) were studied. The authors concluded that statistical models strongly underestimate α emission. A possible reason is that statistical models do not take into account the entrance channel effects in the precompound system, but assume it to be completely thermalized. In this work, we cannot estimate α emission effects, because TDDFT is unable to describe quantum tunneling. However, with the help of the localizations $\mathcal{C}_\alpha$ we can assess the formation of α-cluster effects in the precompound system.

Figure 10 shows snapshots of $\mathcal{C}_\alpha$ in the ^{18}O + ^{12}C reaction at $E_{\rm cm} = 14$ MeV and $b = 2$ fm. Appreciable α clustering effects are apparent, especially at the tips of the precompound system. Our calculations indicate that the tendency for α clusters to appear is strong for energies between 8 and 14 MeV and the impact parameters for which the system fuses. The collision of ^{16}O + ^{12}C reveals a very similar

behavior. While our TDDFT calculations can shed light on the formation process of α clusters, we cannot directly address the experimental data for the α decay cross section and α emission probabilities. Such a task would require significant extensions of the current framework.

V. CONCLUSIONS

We used the time-dependent localization functions $\mathcal{C}_\alpha$ to illustrate cluster effects in TDDFT simulations of the low-energy heavy-ion collisions. Compared to the particle density ρ, the localization $\mathcal{C}_\alpha$ provides excellent measure of clusters of α particles and α-conjugate nuclei appearing in the precompound, or prefission, states produced in nuclear collisions. In this context, Video 2 in the Supplemental Material [49] nicely illustrates the advantage of using $\mathcal{C}_\alpha$ over ρ.

In the central ^{16}O + ^{16}O collision, α and ^{12}C clusters are predicted to be formed. In reactions involving ^{40}Ca, heavier clusters of α-conjugate nuclei are also expected. Moreover, our analysis indicates that the large-amplitude collective motion of the precompound system is far more complex than what is suggested by a naïve liquid drop picture of vibrating nucleonic fluids. Namely, in TDDFT, the resulting collective mode involves cluster motion within quasimolecular configurations, as well as exchange of α particles between clusters, leading to cluster transmutations in heavier systems. Of special interest are the fusion-fission reactions at higher energies, where strong clustering phenomena are predicted both before and after breakup. At this point, a word of caution is in order as, at energies well above the Coulomb barrier, the pure mean-field treatment is not sufficient as two-body collisions become important. A quantitative treatment can be achieved with, e.g., the time-dependent density matrix approach [55,56]. Also, additional terms in the energy density functional can become important [57,58]. However, because in this study we are primarily interested in the qualitative description of cluster effects, we deem the TDDFT treatment as sufficient.

For the collision of ^{16,18}O + ^{12}C we showed that the precompound system has strong tendency to form α clusters. This result supports the conclusions of Ref. [4] that the cluster structure of the initial projectile and target nuclei gives rise to strong entrance channel effects and influences the α emission following fusion. In order to estimate the actual preequilibrium α-emission probability, significant extensions of the formalism by going beyond TDDFT are required. Work along such lines is in progress.

ACKNOWLEDGMENTS

This work was supported by the U.S. Department of Energy under Grants No. DOE-DE-NA0002847 (NNSA, the Stewardship Science Academic Alliances program), No. DE-SC0013365 (Office of Science), No. DE-SC0008511 (Office of Science, NUCLEI SciDAC-3 collaboration), and under BMBF-Verbundforschungsprojekt No. 05P15RDFN1. An award of computer time was provided by the Institute for Cyber-Enabled Research at Michigan State University.

[1] J. R. Birkelund, L. E. Tubbs, J. R. Huizenga, J. N. De, and D. Sperber, Phys. Rep. **56**, 107 (1979).
[2] D. Lebhertz, S. Courtin, F. Haas, D. G. Jenkins, C. Simenel, M.-D. Salsac, D. A. Hutcheon, C. Beck, J. Cseh, J. Darai, C. Davis, R. G. Glover, A. Goasduff, P. E. Kent, G. Levai, P. L. Marley, A. Michalon, J. E. Pearson, M. Rousseau, N. Rowley, and C. Ruiz, Phys. Rev. C **85**, 034333 (2012).
[3] Y. Nagashima, J. Schimizu, T. Nakagawa, Y. Fukuchi, W. Yokota, K. Furuno, M. Yamanouchi, S. M. Lee, N. X. Dai, T. Mikumo, and T. Motobayashi, Phys. Rev. C **33**, 176 (1986).
[4] J. Vadas, T. K. Steinbach, J. Schmidt, V. Singh, C. Haycraft, S. Hudan, R. T. deSouza, L. T. Baby, S. A. Kuvin, and I. Wiedenhöver, Phys. Rev. C **92**, 064610 (2015).
[5] P.-G. Reinhard and E. Suraud, *Introduction to Cluster Dynamics* (Wiley, New York, 2004).
[6] F. Furche and K. Burke, Annu. Rep. Comput. Chem. **1**, 19 (2005).
[7] M. Marques and E. Gross, Annu. Rev. Phys. Chem. **55**, 427 (2004).
[8] *Time-Dependent Density Functional Theory*, edited by M. A. L. Marques, C. A. Ullrich, F. Nogueira, A. Rubio, K. Burke, and E. K. U. Gross, Lecture Notes in Physics Vol. 706 (Springer, Berlin, 2006).
[9] T. Nakatsukasa, K. Matsuyanagi, M. Matsuo, and K. Yabana, Rev. Mod. Phys. **88**, 045004 (2016).
[10] A. Umar and M. Strayer, Phys. Lett. B **171**, 353 (1986).
[11] K.-H. Kim, T. Otsuka, and P. Bonche, J. Phys. G **23**, 1267 (1997).
[12] J. A. Maruhn, P. G. Reinhard, P. D. Stevenson, J. R. Stone, and M. R. Strayer, Phys. Rev. C **71**, 064328 (2005).
[13] A. S. Umar and V. E. Oberacker, Phys. Rev. C **71**, 034314 (2005).
[14] A. S. Umar and V. E. Oberacker, Phys. Rev. C **73**, 054607 (2006).
[15] A. S. Umar, V. E. Oberacker, and C. Simenel, Phys. Rev. C **92**, 024621 (2015).
[16] A. S. Umar, V. E. Oberacker, and C. Simenel, Phys. Rev. C **94**, 024605 (2016).
[17] T. Nakatsukasa and K. Yabana, Phys. Rev. C **71**, 024301 (2005).
[18] C. Simenel, P. Chomaz, and G. de France, Phys. Rev. Lett. **93**, 102701 (2004).
[19] C. Simenel, Eur. Phys. J. A **48**, 152 (2012).
[20] C. Simenel, R. Keser, A. S. Umar, and V. E. Oberacker, Phys. Rev. C **88**, 024617 (2013).
[21] K. Sekizawa and K. Yabana, Phys. Rev. C **93**, 054616 (2016).
[22] B. Schuetrumpf, W. Nazarewicz, and P.-G. Reinhard, Phys. Rev. C **93**, 054304 (2016).
[23] A. S. Umar and V. E. Oberacker, Eur. Phys. J. A **39**, 243 (2009).
[24] V. E. Oberacker, A. S. Umar, J. A. Maruhn, and P.-G. Reinhard, Phys. Rev. C **82**, 034603 (2010).
[25] W. Bauer, G. F. Bertsch, and S. Das Gupta, Phys. Rev. Lett. **58**, 863 (1987).
[26] J. Aichelin, G. Peilert, A. Bohnet, A. Rosenhauer, H. Stöcker, and W. Greiner, Phys. Rev. C **37**, 2451 (1988).

[27] S. Zhang, Y. G. Ma, J. H. Chen, W. B. He, and C. Zhong, Phys. Rev. C **95**, 064904 (2017).
[28] R. R. Betts and A. H. Wuosmaa, Rep. Prog. Phys. **60**, 819 (1997).
[29] C. Beck, R. Nouicer, D. Disdier, G. Duchêne, G. de France, R. M. Freeman, F. Haas, A. Hachem, D. Mahboub, V. Rauch, M. Rousseau, S. J. Sanders, and A. Szanto de Toledo, Phys. Rev. C **63**, 014607 (2000).
[30] C. Beck, J. Phys. Conf. Ser. **436**, 012014 (2013).
[31] S. Y. Kun, A. V. Vagov, and O. K. Vorov, Phys. Rev. C **59**, R585 (1999).
[32] T. L. Belyaeva and N. S. Zelenskaya, Phys. Rev. C **66**, 034604 (2002).
[33] T. Ichikawa, Y. Kanada-En'yo, and P. Möller, Phys. Rev. C **83**, 054319 (2011).
[34] A. S. Umar, J. A. Maruhn, N. Itagaki, and V. E. Oberacker, Phys. Rev. Lett. **104**, 212503 (2010).
[35] A. D. Becke and K. E. Edgecombe, J. Chem. Phys. **92**, 5397 (1990).
[36] P.-G. Reinhard, J. A. Maruhn, A. S. Umar, and V. E. Oberacker, Phys. Rev. C **83**, 034312 (2011).
[37] C. L. Zhang, B. Schuetrumpf, and W. Nazarewicz, Phys. Rev. C **94**, 064323 (2016).
[38] B. Schuetrumpf, C. Zhang, and W. Nazarewicz, in *Nuclear Particle Correlations and Cluster Physics* (World Scientific, Singapore, 2017), Chap. 5, p. 135.
[39] J. A. Maruhn, P.-G. Reinhard, P. D. Stevenson, and A. S. Umar, Comput. Phys. Commun. **185**, 2195 (2014).
[40] M. Kortelainen, J. McDonnell, W. Nazarewicz, P.-G. Reinhard, J. Sarich, N. Schunck, M. V. Stoitsov, and S. M. Wild, Phys. Rev. C **85**, 024304 (2012).
[41] M. Bender, K. Rutz, P. G. Reinhard, and J. A. Maruhn, Eur. Phys. J. A **8**, 59 (2000).
[42] B. Schuetrumpf and W. Nazarewicz, Phys. Rev. C **92**, 045806 (2015).
[43] C. Simenel, Phys. Rev. Lett. **106**, 112502 (2011).
[44] A. Savin, R. Nesper, S. Wengert, and T. F. Fässler, Angew. Chem. Int. Ed. Engl. **36**, 1808 (1997).
[45] A. Scemama, P. Chaquin, and M. Caffarel, J. Chem. Phys. **121**, 1725 (2004).
[46] M. Kohout, Int. J. Quantum Chem. **97**, 651 (2004).
[47] T. Burnus, M. A. L. Marques, and E. K. U. Gross, Phys. Rev. A **71**, 010501 (2005).
[48] J. Poater, D. M., M. Solà, and B. Silvi, Chem. Rev. **105**, 3911 (2005).
[49] See Supplemental Material at http://link.aps.org/supplemental/10.1103/PhysRevC.96.064608 for animations.
[50] P. Christensen, Z. Switkowski, and R. Dayras, Nucl. Phys. A **280**, 189 (1977).
[51] S. L. Tabor, Y. Eisen, D. G. Kovar, and Z. Vager, Phys. Rev. C **16**, 673 (1977).
[52] C. T. Papadopoulos, R. Vlastou, E. N. Gazis, P. A. Assimakopoulos, C. A. Kalfas, S. Kossionides, and A. C. Xenoulis, Phys. Rev. C **34**, 196 (1986).
[53] A. Astier, P. Petkov, M.-G. Porquet, D. S. Delion, and P. Schuck, Phys. Rev. Lett. **104**, 042701 (2010).
[54] D. C. Rafferty, M. Dasgupta, D. J. Hinde, C. Simenel, E. C. Simpson, E. Williams, I. P. Carter, K. J. Cook, D. H. Luong, S. D. McNeil, K. Ramachandran, K. Vo-Phuoc, and A. Wakhle, Phys. Rev. C **94**, 024607 (2016).
[55] M. Tohyama and A. S. Umar, Phys. Rev. C **93**, 034607 (2016).
[56] M. Assié and D. Lacroix, Phys. Rev. Lett. **102**, 202501 (2009).
[57] P. D. Stevenson, E. B. Suckling, S. Fracasso, M. C. Barton, and A. S. Umar, Phys. Rev. C **93**, 054617 (2016).
[58] G. Dai, L. Guo, E. Zhao, and S. Zhou, Sci. China Phys. Mech. Astron. **57**, 1618 (2014).